

The Shape and Orientation of NGC 3379: Implications for Nuclear Decoupling

Thomas S. Statler

Department of Physics and Astronomy, Ohio University, Athens, OH 45701, USA; tss@coma.phy.ohio.edu

ABSTRACT

The intrinsic shape and orientation of the elliptical galaxy NGC 3379 are estimated by dynamical modeling. The maximal ignorance shape estimate, an average over the parameter space, is axisymmetric and oblate in the inner parts, with an outward triaxiality gradient. The 1σ limits on total-mass triaxiality T are $T < 0.13$ at 0.33 kpc and $T = 0.08 \pm 0.07$ at 3.5 kpc from the center. The luminous short-to-long axis ratio $c_L = 0.79^{+0.05}_{-0.1}$ inside 0.82 kpc, flattening to $c_L = 0.66^{+0.07}_{-0.08}$ at 1.9 kpc. The results are similar if the galaxy is assumed to rotate about its short axis. Estimates for c_L are robust, but those for T are dependent on whether the internal rotation field is disklike or spheroid-like. Short-axis inclinations i between 30° and 50° are preferred for nearly axisymmetric models; but triaxial models in high inclination are also allowed, which can affect central black hole mass estimates. The available constraints on orientation rule out the possibility that the nuclear dust ring at $R \approx 1.5''$ is in a stable equilibrium in one of the galaxy's principal planes. The ring is thus a *decoupled nuclear component* not linked to the main body of the galaxy. It may be connected with ionized gas that extends to larger radii, since the projected gas rotation axis is near the minor axis of the ring. The gas and dust may both be part of a strongly warped disk; however, if caused by differential precession, the warp will wind up on itself in a few 10^7 years. The decoupling with the stellar component suggests that the gas has an external origin, but no obvious source is present.

Subject headings: galaxies: elliptical and lenticular, cD—galaxies: individual (NGC 3379)—galaxies: kinematics and dynamics—galaxies: structure

1. Introduction

Like many astronomers, the “standard elliptical galaxy” NGC 3379 appears outwardly normal but, deep inside, has serious issues. To the casual observer this object is as ordinary as can be. Its optical surface brightness distribution follows an $r^{1/4}$ law over a span of 10 magnitudes (de Vaucouleurs & Capaccioli 1979). Its isophotes are almost perfectly elliptical and aligned (Peletier et al. 1990). Its optical colors are typical of an old population, and color gradients are small (Goudfrooij et al. 1994). It rotates slowly about its apparent minor axis (Davies & Illingworth 1983, Davies & Birkinshaw 1988). It shows no sign of current or past interactions (Schweizer & Seitzer 1992), and contains only a tiny amount of detectable interstellar matter, seen only in H α +[N II] emission (Macchetto et al. 1996) and dust absorption (van Dokkum & Franx 1995, Michard 1998).

On closer examination, the photometric and kinematic structure of the galaxy are puzzling. Deviations of the surface brightness profile from the $r^{1/4}$ law, though small, are significant (Capaccioli et al. 1987). Based on photometric similarities to NGC 3115, Capaccioli et al. (1991) propose that NGC 3379 is a highly triaxial S0 galaxy seen at low (31°) inclination. The orientation and shape of the galaxy are difficult to constrain, however. Van der Marel et al. (1990), using stellar kinematic data and explicitly axisymmetric

models, infer an inclination of 60° , at which the galaxy would be intrinsically almost as round as it appears. Statler (1994c, hereafter S94) considers triaxial models, introducing a methodology that relies on multi-position-angle observations of the mean velocity field. These models rule out the axis ratios advocated by Capaccioli et al. (1991) at 98% confidence,¹ but allow a wide variety of flattened nearly axisymmetric, or rounder triaxial shapes, and a correspondingly wide variety of inclinations.

Detailed kinematic studies of both stars (Bender, Saglia, & Gerhard 1994; Statler & Smecker-Hane 1999, hereafter SS99) and planetary nebulae (Ciardullo, Jacoby, & Dejonghe 1993) show a richer kinematic structure than one might have expected from older data. Inflections in the rotation and dispersion profiles are suggestive of a two-component structure, and are similar to those of S0 galaxies (Fisher 1997). SS99 suggest a low (30°) inclination and a *weakly* triaxial S0-like shape on the basis of these similarities. At large radii the stellar dispersion profile joins with that of the planetary nebulae, which is consistent with a *constant* mass-to-light ratio out to $r \approx 10$ kpc (Ciardullo, Jacoby, & Dejonghe 1993).

More recently, the nuclear regions of NGC 3379 have caught the attention of a number of workers, particularly as a likely home for a supermassive black hole. Kinematic data from the ground and from *HST* imply a central mass in the vicinity of $10^8 M_\odot$ (Magorrian et al. 1998; Gebhardt et al. 2000a, hereafter G00), placing it roughly in the middle of the $M_{\text{BH}}-L_{\text{bulge}}$ (Magorrian et al. 1998) and $M_{\text{BH}}-\sigma_{\text{bulge}}$ (Ferrarese & Merritt 2000, Gebhardt et al. 2000b) correlations, but the black hole mass is dependent, to within factors of order unity, on the orientation of the galaxy. The nuclear dust ring (G00, Pastoriza et al. 2000, hereafter P00) seen on arcsecond scales and the slightly more extended H α +[N II] emission (Macchetto et al. 1996, P00) might be useful in constraining the orientation, if it could be assumed that the interstellar material were in an equilibrium configuration in one of the galaxy’s principal planes. However, there seems not to be compelling justification for such an assumption, since the apparent principal axes of the dust and ionized gas are aligned neither with the stellar principal axes nor with each other. Figure 1 shows a sketch of these components and their relation to the starlight.

In this paper, I revisit the problem of constraining the shape and orientation of the main body of NGC 3379, using the newest stellar kinematic data (SS99, Gebhardt & Richstone 2000). The approach follows that of S94, as modified by Statler, Dejonghe, & Smecker-Hane (1999, hereafter SDS). The data are of sufficiently high quality to attempt to recover not just an average shape, but the shape *profile* over a full decade in radius. The presentation is arranged as follows: Section 2 describes the photometric and kinematic data used in the modeling. Section 3 gives an overview of the method, and details where the present treatment differs from previous applications. Sections 4 and 5 describe the results for the estimates of the intrinsic shape profile and the orientation, respectively. Section 6 discusses the implications of the results for the structure and evolution of NGC 3379’s nuclear regions, and Section 7 restates the major conclusions.

2. Observational Data

The handling of the observational material parallels that in earlier work. Kinematic data consist of mean velocities measured along several long-slit cuts through the galaxy center. Data for P.A.’s 205, 250, 295, and 340 come from SS99; their published velocities for $6'' \leq R \leq 78''$ are reflected about the center and then averaged over pairs of adjacent bins, giving 9 annular zones of mean radius $6''.6$, $9''.0$, $11''.4$, $13''.8$, $16''.2$, $19''.8$, $26''.4$, $38''.4$, and $69''.0$. Data inside $6''$ are not used because the models perform poorly in regions where

¹The model of Capaccioli et al. is not internally consistent due to unfortunate trigonometric errors (S94, § 5.2).

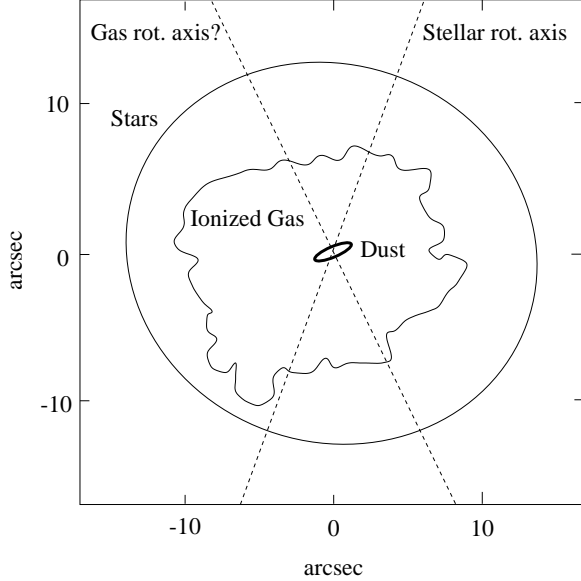


Fig. 1.— Sketch of the central regions of NGC 3379, oriented with North at the top and East at left. A typical stellar isophote is shown by the big ellipse. The apparent rotation axis of the stars coincides very closely with the morphological minor axis, shown as the thick dotted line. The convoluted outline shows the outermost H α +N II isophote plotted by Machetto et al. (1996). The gas rotation is measured only within 3'' of the center, and the rotation axis is poorly determined. Gas kinematics are consistent with the rotation axis lying along the apparent minor axis (light dotted line) of the central dust ring (thick ellipse). Both the stellar and gas velocity fields are such that the right side of the figure is at positive velocities and the left side at negative.

the rotation curve is steeply rising. Additional data for P.A.'s 180, 225, and 235 are taken from Gebhardt & Richstone (2000) and linearly interpolated onto the same radial scale.

Ellipticities and major axis position angles are drawn from the R band photometry of Peletier et al. (1990) and averaged over the same radial bins used for the kinematic data, weighted by the inverse square of the published errors. The adopted errors in the rebinned data represent the larger of the mean observational error per data point and the standard deviation in the bin.

The complete set of observational data used in the modeling is summarized in Table 1.

3. Models and Methods

3.1. Thumbnail Sketch

The shape-fitting method and the models on which it is based have been described exhaustively in earlier papers (Statler 1994a, Statler & Fry 1994, Statler 1994b, hereafter Papers I, II, and III; S94, SDS). The method finds, in a probabilistic sense, the boundaries between the major circulating orbit families using the 2-dimensional radial velocity field and its alignment with the surface brightness distribution. The locations of these boundaries and the apparent shape of the galaxy then constrain the underlying 3-dimensional mass distribution. The analysis of the velocity field proceeds by comparison with dynamical models, which are constructed by solving the equation of continuity for the mean stellar velocities using confocal streamlines linked to the triaxiality T of the total mass distribution. The triaxiality is defined in terms of the axis

TABLE 1. Photometric and Kinematic Data Used in Shape Fitting

R	ϵ	P.A. _{·maj}	v_{180}	v_{205}	v_{225}	v_{235}	v_{250}	v_{295}	v_{340}
6''.6	$0.074 \pm .001$	$74^\circ 4 \pm 0^\circ 5$	13.4 ± 7.5	23.3 ± 2.0	25.2 ± 5.5	41.9 ± 9.2	35.8 ± 1.5	26.6 ± 1.5	3.7 ± 1.5
9''.0	$0.074 \pm .001$	$73^\circ 5 \pm 0^\circ 9$	9.1 ± 5.0	22.8 ± 1.7	39.0 ± 6.9	44.6 ± 7.4	40.6 ± 1.7	30.0 ± 1.7	1.4 ± 1.7
11''.4	$0.075 \pm .001$	$72^\circ 3 \pm 0^\circ 8$	11.4 ± 5.0	27.4 ± 1.9	33.0 ± 6.1	38.1 ± 6.1	43.8 ± 1.9	29.1 ± 2.0	5.5 ± 1.9
13''.8	$0.077 \pm .001$	$71^\circ 2 \pm 1^\circ 0$	12.0 ± 5.0	27.9 ± 2.2	34.8 ± 6.4	44.8 ± 6.0	48.6 ± 2.2	30.8 ± 2.2	2.3 ± 2.3
16''.2	$0.079 \pm .003$	$70^\circ 2 \pm 0^\circ 5$	12.6 ± 5.0	37.6 ± 6.9	52.1 ± 6.0	30.3 ± 2.6	53.0 ± 2.5	36.4 ± 2.6	3.0 ± 2.6
19''.8	$0.087 \pm .009$	$70^\circ 0 \pm 0^\circ 4$	8.6 ± 5.6	30.4 ± 2.5	43.6 ± 11.4	56.0 ± 7.2	55.3 ± 2.6	29.5 ± 2.6	1.0 ± 3.0
26''.4	$0.106 \pm .012$	$69^\circ 9 \pm 0^\circ 3$	10.6 ± 6.0	31.5 ± 2.8	45.0 ± 13.7	53.1 ± 8.8	52.4 ± 3.0	33.9 ± 3.0	-3.8 ± 3.2
38''.4	$0.129 \pm .005$	$69^\circ 9 \pm 0^\circ 4$	7.4 ± 8.1	29.7 ± 3.1	39.2 ± 10.4	46.5 ± 11.0	55.0 ± 3.5	39.6 ± 3.5	-3.7 ± 3.9
69''.0	$0.129 \pm .004$	$70^\circ 2 \pm 0^\circ 7$	-22.9 ± 20.0	25.5 ± 6.3	61.7 ± 25.0	104.8 ± 44.0	44.9 ± 7.4	30.3 ± 6.0	1.7 ± 7.5

ratios of the equidensity surfaces by $T \equiv (1 - b^2)/(1 - c^2)$, where b and c are the middle-to-long and short-to-long axis ratios, respectively; corresponding axis ratios for the luminosity distribution are labeled by b_L and c_L . The major assumption of the models is that rotation of the galaxy arises from internal streaming in a non-rotating potential. Certain other simplifying assumptions are made to facilitate the projection along the line of sight. The models include a number of adjustable parameters, which allow a wide array of dynamical configurations to be computed efficiently. These parameters are described in Paper I, and collectively abbreviated by \mathbf{d} .

The statistical estimate of the shape or orientation of the galaxy is obtained by Bayesian methods. Computing a large grid of models results in a multidimensional likelihood function $L(T, c_L, \Omega, \mathbf{d})$ in the space of shape (T, c_L) , orientation Ω , and dynamical parameters \mathbf{d} . The likelihood is multiplied by a prior, or model parent distribution, which is isotropic in orientation, but which may reflect assumptions about the dynamics. The product is integrated over all unwanted parameters to give a posterior probability distribution for the parameters of interest. A shape estimate is thus a probability density $P(T, c_L)$. As in earlier work it is assumed that the isodensity surfaces of mass and luminosity have the same shape at the same radii; tests in Paper III showed that the distribution in (T, c_L) is still robust when this assumption is mildly violated.

The 9 annular zones of the galaxy are initially modeled independently, then combined assuming that the galaxy's principal axes are intrinsically aligned throughout (see Appendix A of SDS). If it is explicitly assumed that the triaxialities of the luminous and total mass distributions are the same, then the shape profile can also be required to reproduce the observed isophotal twist (which is small in this case). Except where specifically noted, all of the results in this paper include the isophotal twist constraint, but are not significantly altered by ignoring it.

3.2. Modifications to the Basic Procedure

3.2.1. Model Grid

A preliminary set of models shows that, as in earlier work, the results for NGC 3379 are very insensitive to the parameters k and l , which describe the radial dependence of luminosity density and mean rotation assumed in the projection integrals (see Paper I, equation [32]). Rather than use a grid of values for each parameter as in previous cases, I simply fix the values at $k = 3$, $l = 0$ for the final modeling.

The same preliminary models show a complicated dependence on the function $v^*(t)$, which describes the latitude dependence of the mean streaming velocity across the x - z plane.² The variable t is a scaled latitude, defined (equation [9] of Paper II) so that $t = 0$ and $t = 2$ correspond to the x and z axes, respectively, and the boundary between short-axis and long-axis tube orbits³ is at $t = 1$. In previous papers, $v^*(t)$ in each interval was assumed to be either constant or linearly decreasing to zero at $t = 1$, as shown by the heavy lines in Figure 2a; these limiting cases are referred to as “spheroid-like” and “disklike” rotation. For NGC 3379, I find it necessary to include the intermediate cases. Again, I take $v^*(t)$ to be linear in each interval, with maxima at $t = 0$ and $t = 2$, decreasing to $(\frac{1}{4}, \frac{1}{2}, \frac{3}{4})$ of the maximum at $t = 1$; these functions are shown as the light lines in Figure 2a. To aid intuition, Figure 2b shows how these choices translate into the actual latitude dependence of the velocity, for streaming about the short axis in an oblate axisymmetric

²The x , y , and z axes correspond to the long, middle, and short axes of the model.

³For brevity I also use the synonyms “Z tubes” and “X tubes.”

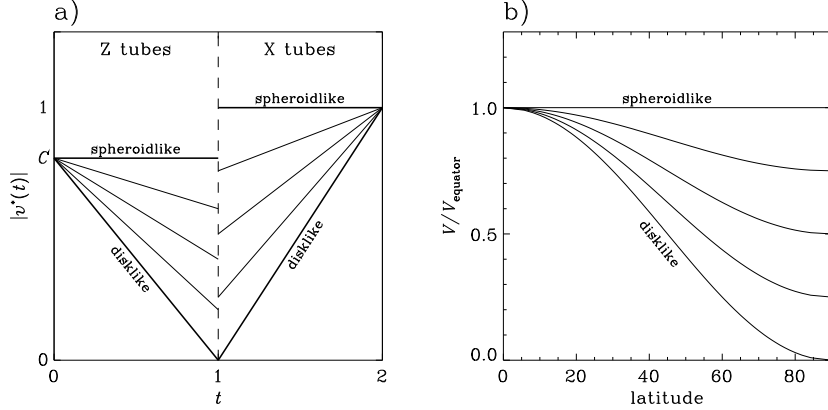


Fig. 2.— (a) Adopted forms for the $v^*(t)$ function, which gives the mean internal velocity crossing the x - z plane as a function of a scaled latitude t . The x and z axes correspond to $t = 0$ and $t = 2$, respectively; $t = 1$ marks the boundary between short-axis and long-axis tubes. *Heavy lines* show the extreme disklike and spheroid-like cases used in earlier work; *light lines* show the intermediate cases added for the present models. (b) Translation of $v^*(t)$ for short-axis tubes in an axisymmetric oblate model into true mean velocity as a function of latitude above the equatorial plane.

model. Note that in a triaxial model the character of the long and short axis streaming can be completely independent.

3.2.2. Penalty for Steep Shape Gradients

Combining the separate annular fits as prescribed in SDS effectively merges the 9 annuli as if they were separate galaxies seen from the same direction. This prescription ignores the physical constraint that the axis ratios of the isodensity surfaces should change continuously—and, for *bona fide* ellipticals, slowly—with r . To remedy this I introduce a set of penalty factors of the form

$$\exp \left[-\frac{(T_{i+1} - T_i)^2 + (c_{L,i+1} - c_{L,i})^2}{2\sigma_g^2} \right] \quad (1)$$

for each pair of adjacent annuli ($i = 1, \dots, 8$), with the constant $\sigma_g = 0.118$. This choice implies that a complete change of shape (i.e., oblate to prolate, or sphere to disk) between the innermost and outermost annuli would be penalized as *a priori* unlikely at the 4σ level.

3.2.3. Parent Shape Distribution

In previous papers a flat prior distribution in (T, c_L) was adopted for modeling individual systems. However, a realistic estimate of the parent shape distribution has now been presented by Bak & Statler (2000, hereafter BS), derived from the 13-galaxy Davies & Birkinshaw (1988) sample, which includes NGC 3379. BS show that their “maximal ignorance” distribution, obtained from an unweighted sum over all parameters \mathbf{d} , gives an ellipticity distribution completely consistent with the 165-galaxy compilation of Ryden (1992). For this work I adopt the BS maximal ignorance result (their Figure 2a) as the prior shape distribution.

4. Intrinsic Shape

Formally, the shape profile for the galaxy is a joint probability distribution in 18 variables. To make this more manageable, I follow SDS and project the distribution into the (T, c_L) plane for each annulus. The resulting 9 marginal distributions are estimates of the mean shape in each annulus, using the data from all radii but independent of the actual shapes of the other annuli. Figure 3 shows four representative results. Each small panel shows the (T, c_L) plane, with oblate spheroids at the right edge, prolate spheroids at the left edge, and spheres at the top. The marginal posterior density $P(T, c_L)$ is displayed on a linear color scale, with contours enclosing the 68% and 95% highest posterior density (HPD) regions. Each column shows one complete shape profile, with the mean radii of the 9 annuli indicated along the far right margin. The columns differ in the assumed prior distribution in the dynamical parameters \mathbf{d} .

The small ellipticity and the symmetric, well-aligned velocity field of NGC 3379 make it, ironically, a difficult object to model. Broadly speaking, there are three types of models that fit the data (though there are no clear divisions and so this trichotomy is artificial): (1) fairly round models with small but nonzero triaxiality, seen at moderate inclination; (2) somewhat flatter nearly oblate models, seen at lower inclination; and (3) highly triaxial models with lines of sight in the x - z plane. The first group of models is the most successful, and dominates the total probability in an unweighted sum over all models. This sum gives the maximal ignorance estimate, shown in the first column of Figure 3. In this estimate, the galaxy is most probably axisymmetric at small radii, and shows a slight increase in triaxiality and flattening toward larger R . The contribution from the second group of models can be seen as the weaker second peak near $T \approx 0.07$ for $R < 20''$, and the third group is responsible for the tenuous tail extending toward $T = 0.5$. The second column of Figure 3 shows the shape estimate under the assumption of zero intrinsic kinematic misalignment, i.e., rotation purely about the short axis. This result is obtained by omitting models with net rotation in the X tube orbits. The most probable shape at each radius agrees fairly closely with that in the maximal ignorance result, with a slightly larger outward triaxiality gradient. The tail toward large T is more prominent, but contains a small fraction of the total probability. Both this and the maximal ignorance result imply that NGC 3379 is weakly triaxial and probably close to oblate.

The third group of models becomes particularly problematic in some parts of the \mathbf{d} parameter space. For lines of sight near the x - z plane, the apparent kinematic misalignment is always small, and one can freely vary the axis ratios while preserving the projected shape, without moving the apparent rotation axis. A model of almost any triaxiality can be made to fit the data in such an orientation by fine-tuning the $v^*(t)$ function (Fig. 2). As a result, restricting the dynamical prior to certain regions of parameter space can give very different answers for the inferred triaxiality. Two extreme cases are shown in the third and fourth columns of Figure 3. In the third column, the models are restricted to those in which the rotation in Z tubes is moderately spheroid-like, corresponding to the second line from the top in the left half of Figure 2. No constraint is put on the X tubes. The result is dominated by prolate-triaxial models viewed in the x - z plane. In the fourth column, the aligned-rotation models from the second column are restricted only to those with disklike rotation. The disappearance of the distribution's large- T tail confirms that spheroid-like rotation makes the highly triaxial models viable.

To help in understanding the radial shape profiles, I project the distributions in Figure 3 onto the T and c_L axes and plot the 1-dimensional marginal distributions against r . Figure 4 shows the profiles of T and c_L for the same four cases shown in Figure 3. The plotted points connected by solid lines show the most-probable values (i.e., peaks of the marginal distribution), and the dashed and dotted lines indicate crossings of the 68% and 95% HPD levels. The radial scale has been set using a distance of 10.4 Mpc (Ajhar

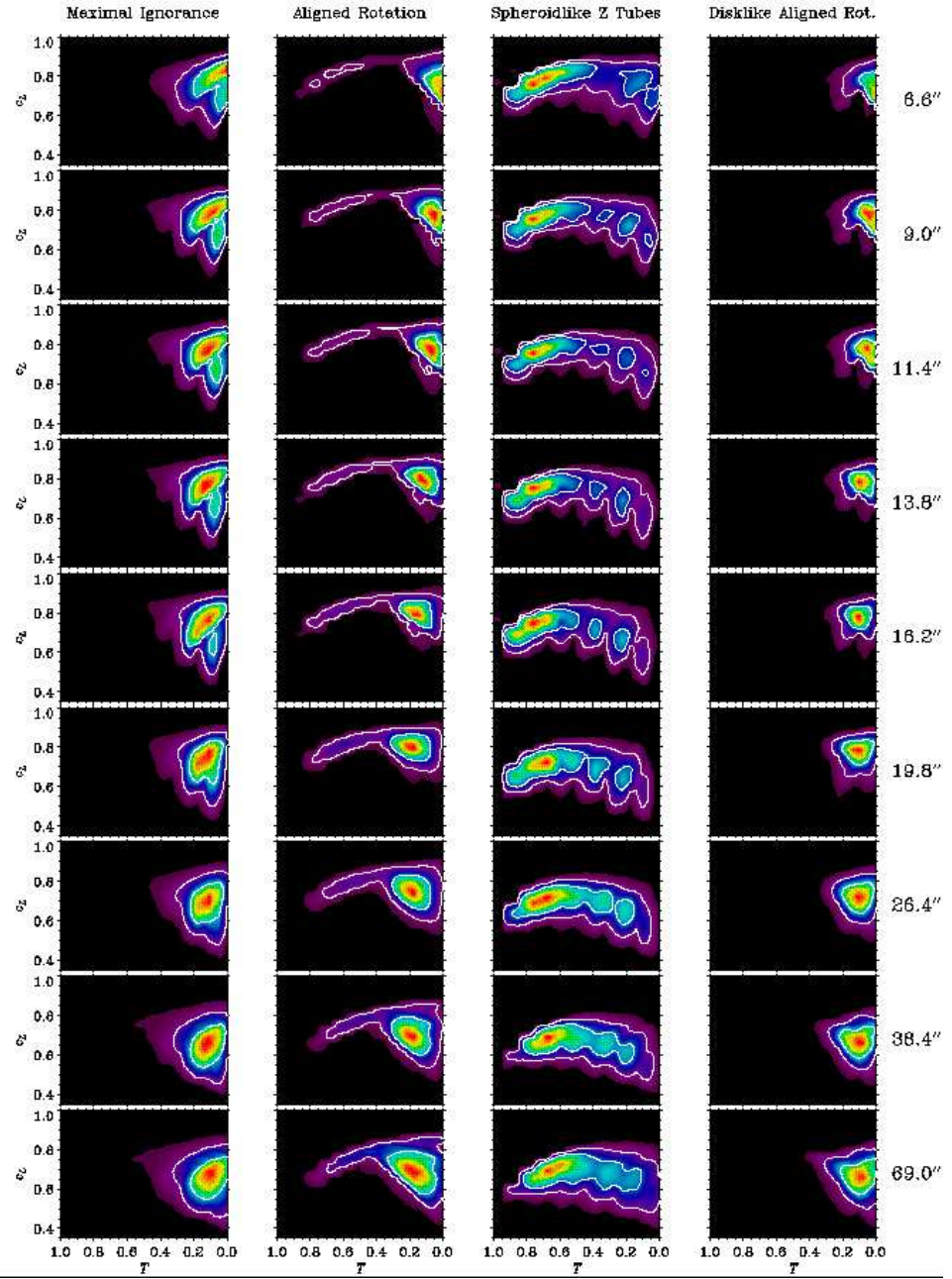


Fig. 3.— Shape profile estimates for NGC 3379. Each column shows an estimate using a different dynamical prior; each small panel shows the Bayesian probability in total mass triaxiality T and luminous axis ratio c_L at one radius (labeled at far right). Contours mark the 68% and 95% highest posterior density (HPD) regions. *First column:* maximal ignorance estimate, an unweighted average over the dynamical parameter space. *Second column:* estimate using only models that rotate about their short axes. *Third column:* estimate with spheroid-like rotation in Z tubes (see § 4 of text). *Fourth column:* estimate using only models with disklike rotation about their short axes.

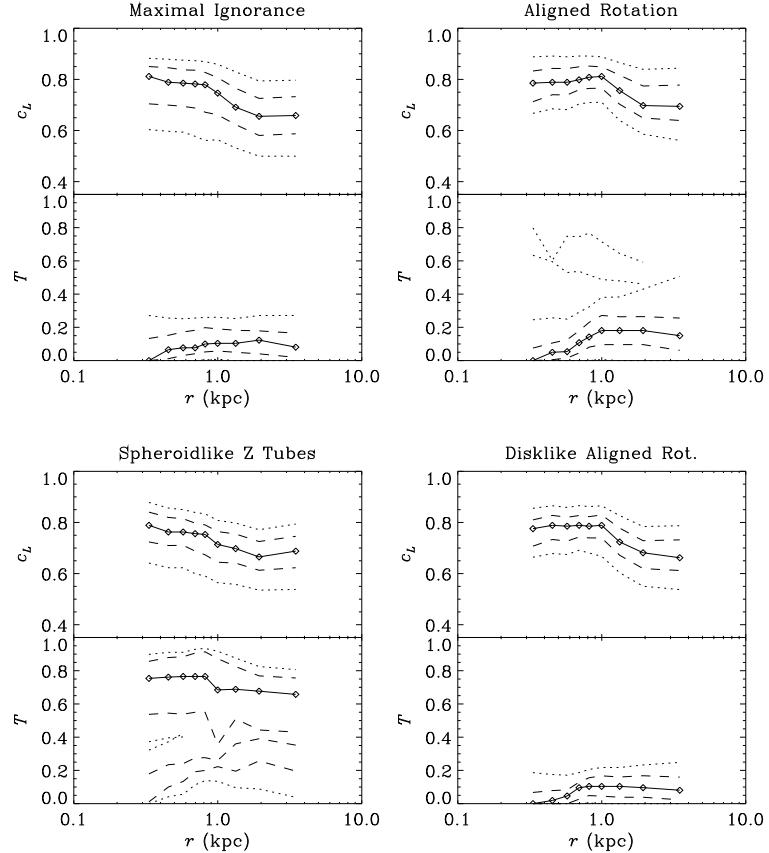


Fig. 4.— Radial profiles of triaxiality and flattening for the same four cases shown in Fig. 3. Profiles are determined from 1-dimensional marginal distributions, hence these are not joint (T, c_L) profiles. *Points and solid lines*, maximum-posterior-probability values; *dashed lines*, crossings of the 68% HPD level (1σ error region); *dotted lines*, crossings of the 95% HPD level (2σ error region).

et al. 1997). One can easily see the tendency for outwardly-increasing triaxiality in 3 out of 4 cases, as well as the effect of altering the dynamical prior. Even though the maximal ignorance result gives a formally narrow error region, the systematic uncertainties associated with disklike or spheroid-like rotation are large in comparison; in other words, the triaxiality profile is *prior dominated*, and should not be considered a robust result. On the other hand, the radial run of the short-to-long axis ratio c_L is robust, and not sensitive to the dynamical prior. The maximal ignorance profile is flat or slowly declining for $r \lesssim 1$ kpc, then changes over a factor ~ 2 in radius from the inner value of $c_L \approx 0.8$ to an outer value $c_L \approx 0.7$. This transition is driven primarily by the photometric ellipticity gradient, though modulated by kinematics, and occurs more abruptly in the models that rotate purely about their short axes.

5. Orientation

A different projection through the parameter space can give a probability distribution for the orientation of NGC 3379. The central points of interest here are the inclination of the (probably axisymmetric) inner

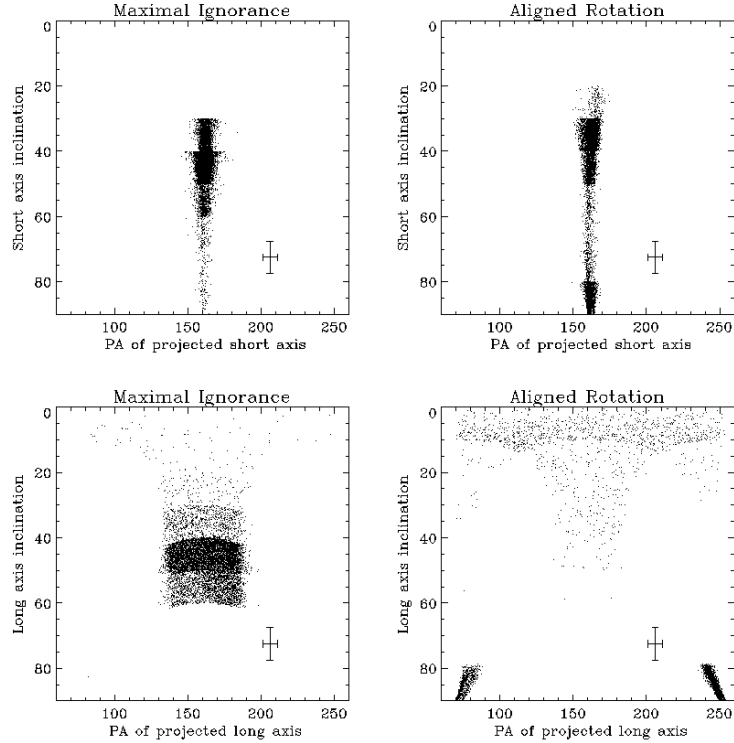


Fig. 5.— *Top row*: Joint distribution in short axis inclination to the line of sight and projected short axis position angle, for (*left*) maximal ignorance and (*right*) rotation about the short axis. *Error bars* mark the orientation required if the nuclear dust ring is assumed to lie in the plane normal to the short axis. Horizontal banding reflects the coarse (10°) angular grid in the polar angle θ . *Bottom row*: Same, but for the orientation of the long axis; *error bars* mark the orientation required if the dust ring is assumed normal to the long axis.

region and the relation of the stars to the nuclear dust ring (Figure 1). The ring has a semi-major axis of approximately $1''.5$, with the minor axis along P.A. 206 ± 5 , roughly 45° away from the minor axis of the starlight. If the ring is circular, its aspect ratio indicates that its symmetry axis is inclined to the line of sight by $73^\circ \pm 5^\circ$.

In a non-tumbling triaxial potential, a massless ring can be stable in the planes normal to the long or short axes.⁴ The latter case would seem the more likely, if the ring dynamics are coupled to the stellar dynamics. This would require P.A. 206 to correspond to the direction of the projected short axis, and a 73° inclination of this axis to the line of sight. In the top two panels of Figure 5 I show joint probability distributions in projected short axis P.A. and short axis inclination calculated from the models, for the maximal ignorance and aligned rotation cases. A rejection method has been used to populate the particle-density plots. The inclination is not well constrained, but the P.A. of the projected short axis lies within $\pm 10^\circ$ of the apparent minor axis, at better than 3σ confidence. The error bars show the orientation required if the dust ring were normal to the short axis; it is clear that this configuration is not viable.

⁴A tumbling rate sufficient to create a significantly tilted equilibrium for the nuclear ring would place corotation well within the main body of the galaxy, so this case is excluded.

One might be concerned that this result could be altered if the luminous and total-mass triaxialities were different, in which case constraining the mass triaxiality profile to reproduce the observed isophotal twist would be inappropriate. Removing this constraint widens confidence intervals on the projected short axis P.A. by about 50%, but the basic result is unchanged.

It is worth reiterating that the short-axis inclination is not well constrained by the data, even though the flattening is fairly well determined. This can be a counterintuitive result, if one's intuition is based on axisymmetric models. Even a weakly triaxial model does not project to a given apparent shape at a unique inclination. Since T is poorly constrained, the inclination is as well, and suffers from the same systematic uncertainties. Modelers are cautioned not to think of the inclination as being set by the short-to-long axis ratio. This is a valid inference only if one asserts via an *ad hoc* prior that the galaxy is axisymmetric.

If the dust ring were normal to the long axis, then this axis would have to fall at P.A. 206 in projection and lie at the right inclination. The bottom row of Figure 5 shows the results from the models. The constraints are much weaker than for the short axis, and also more dependent on the dynamical prior. However, the distributions shown are typical in that different subsets of the \mathbf{d} parameter space do not populate regions of the figure that are unpopulated in these examples. The same is true for models in which the isophotal twist constraint is lifted. The orientation required by the dust lane falls squarely in an unpopulated region; I conclude that a configuration with the ring about the long axis is also ruled out.

The last equilibrium refuge for the dust lies in making the galaxy exactly axisymmetric in the inner parts and placing the dust in a polar ring at the correct azimuth, where it would be neutrally stable. From the *HST* photometry of G00, the ellipticity just outside the ring is 0.11, and the minor axis P.A. is 161° , which must equal the P.A. of the projected short axis. To match the observed ring orientation and aspect ratio requires the short axis to be inclined 24° to the line of sight. At this inclination all oblate objects—even razor-thin disks—project to ellipticities < 0.11 . On the other hand, the required inclination is very sensitive to the ring parameters; pushing both the ring P.A. and inclination by 1σ in the favorable directions changes the galaxy's inclination to 33° , at which a flattening of $c_L = 0.54$ will project to the correct ellipticity. Pushing by 1.5σ in both directions allows $c_L = 0.66$ to fit the inner photometry at an inclination of 38° , which is well within the viable region for oblate models found in Section 4. A polar ring configuration is therefore not ruled out.

6. Discussion

By fitting dynamical models to the stellar kinematics and photometry, I have shown that NGC 3379 is most probably axisymmetric and oblate in its inner parts, with a weak but significant outward triaxiality gradient.⁵ There are, however, regions of parameter space where the best models are prolate-triaxial. Thus the estimate of small triaxiality is dependent on the dynamical prior, and, pending a better understanding of the internal velocity fields of ellipticals, should not be considered robust.

Nonetheless, this result bolsters the use of oblate axisymmetric models for constraining the mass of the putative central black hole (Magorrian et al. 1998, G00). Even though the present models use data only from $R > 6''$, there is no sign of serious photometric (G00) or kinematic (SS99) twists interior to this radius

⁵ It is worth noting that this gradient is required both by the observed isophotal twist and by the twist of the velocity field, which are in opposite directions (see Fig. 6a of SS99). Relaxing the requirement that the models match the isophotal twist gives the same T gradient as that in the top row of Fig. 4, but at lower significance.

that could signal a loss of axisymmetry. If axisymmetry is asserted *a priori*, and the axis ratios assumed constant from $R = 6''$ inward, the maximal-ignorance flattening $c_L = 0.81^{+0.05}_{-0.1}$ would imply an inclination of $40^{+8}_{-4}^\circ$. At this inclination, the models of G00 imply a central dark mass of $2 \times 10^8 M_\odot$. At the same time, one must be conscious of the highly triaxial solutions, particularly those at high inclinations, which would imply smaller central masses than the less-inclined axisymmetric models. G00’s best-fit black hole mass drops by a factor of 2 as they tilt their oblate models from 50° to 90° (their preferred inclination). In addition, triaxial systems observed down their long axes can appear atypically “hot” because of velocity anisotropy, requiring less dark mass for a given observed dispersion if triaxiality persists to small radii.

The present results for the shape of NGC 3379 are consistent with those found earlier using older kinematic data (S94, Fig. 8; BS, Fig. 4). On the other hand, they do not strongly favor the argument of SS99 that the galaxy is a weakly triaxial, slightly puffy S0-like system seen at low inclination. SS99 make this argument based on photometric and kinematic similarities with NGC 3115 (Capaccioli et al. 1991, Fisher 1997). In the present models, configurations that are highly flattened ($c_L < 0.5$) and nearly oblate are viable and do contribute to the total probability density, but only at a low level. Moreover, their contribution comes almost entirely from the most spheroidlike models, whereas one would expect more disklike rotation if the galaxy were a two component disk-bulge system. Alternatively, if one *believes* that the nuclear dust is in a polar ring, this configuration requires an inclination $< 43^\circ$ (3σ confidence), consistent with that argued for by SS99.

But there is no compelling reason for the dust ring to be polar. The evolution of such an object is not like the evolution of the large polar rings commonly observed (e.g., Whitmore et al. 1990) and modeled (e.g. Sackett et al. 1994). A nuclear ring is immersed in the rotating stellar population, and will be torqued by dynamical friction. One should expect a nuclear polar ring to secularly tilt out of the meridional plane and begin to differentially precess in the oblate potential. Big polar rings can be stabilized by self gravity (Sparke 1986, Arnaboldi & Sparke 1994), but this is not an option for the NGC 3379 ring, which obscures only $\sim 1\%$ of the galaxy’s V -band surface brightness. Assuming a Galactic dust-to-gas ratio, this A_V implies a mass only of order $100 M_\odot$, compared with the $\sim 10^8 M_\odot$ enclosed by the ring.

Regardless of whether the nuclear ring is strictly polar or merely misaligned with the symmetry axes, the results of Section 5 show clearly that it is effectively decoupled from the main body of the galaxy. This echoes the original finding of Davies & Birkinshaw (1988) of a lack of correlation between the radio and optical axes of radio ellipticals. In general, recent imaging studies (van Dokkum & Franx 1995, Carollo et al. 1997) have found a bewildering variety of nuclear dust morphologies in ellipticals, which seem totally uncorrelated with properties of the host galaxies. For NGC 3379, the observed dust surely cannot have come directly from the stellar population, whose mass distribution and angular momentum are extremely well ordered and not aligned with the dust ring. For one of the most ordinary and quiescent ellipticals in the sky to contain a misaligned—and, presumably, rapidly evolving—non-stellar component is remarkable.

The nature and history of the dust ring may be related to the ionized gas that extends from the center out to $R \approx 8''$ (Figure 1; Macchetto et al. 1996). P00 obtain $\text{H}\alpha + [\text{N II}]$ rotation curves for $R \lesssim 3''$ along P.A. 70, 115, and 160. The maximum observed velocity is approximately 220 km s^{-1} on P.A. 70 and 115, and roughly half this on P.A. 160, which is the stellar minor axis. These amplitudes are consistent with the gas rotation axis lying parallel to the axis of the dust ring. From the very round $\text{H}\alpha + [\text{N II}]$ isophotes and an assumption that the gas distribution is circular, P00 infer an inclination of 25° for the ionized disk. However, this inclination implies gas rotation velocities in excess of 500 km s^{-1} , which seems unrealistic considering the $\sim 200 \text{ km s}^{-1}$ dispersion of the stars.

More likely, the ionized gas lies in a strongly warped disk, in which case the outer H α +[N II] isophotes may not reflect the disk's inclination at the smaller radii where P00 measure the rotation. The dust ring could then be part of the same structure, either marking the inner edge of the disk or merely made prominent by its low inclination. Macchetto et al. estimate the ionized disk to be only a few $10^3 M_\odot$ in mass. It is far from clear whether a low mass, low density warped disk could be a long-lived object. In a slightly oblate isothermal system with velocity dispersion σ , inclined, nearly circular orbits of radius r precess at a frequency given in the epicycle approximation by

$$\omega_p = \frac{\sqrt{2}\sigma}{r} \left(\frac{1}{q} - 1 \right), \quad (2)$$

where q is the flattening of the potential (Statler et al. 1996). The preferred flattening $c_L = 0.8$ gives $q = 0.93$ if mass follows light, from which the precession period is

$$\frac{2\pi}{\omega_p} \approx 14 \left(\frac{R}{1''} \right) \text{ Myr.} \quad (3)$$

To warp an initially coplanar disk by 90° between $R = 1''$ and $R = 5''$ by differential precession thus requires only about 4 Myr. Significantly later than this, say, by 20 Myr, the disk will have evolved into a multiply-wrapped sheet, which may be inconsistent with the observed velocity field. This simple calculation ignores the effect of dynamical friction against the stars, which will simultaneously try to align the disk's angular momentum with the stellar rotation axis.

7. Conclusions

Dynamical models have been fit to the stellar kinematics and surface photometry of NGC 3379, in order to constrain the intrinsic shape profile and orientation of the main body of the galaxy. The Bayesian “maximal ignorance” shape estimate, which reflects an unweighted average over the dynamical parameter space, indicates that the galaxy is most probably axisymmetric and oblate in its inner parts, with a slight but significant outward triaxiality gradient. The formal 1σ limits on triaxiality T are $T < 0.13$ at $R = 6''.6$ (0.33 kpc) and $T = 0.08 \pm 0.07$ at $R = 69''$ (3.5 kpc). The most probable short-to-long axis ratio of the luminosity distribution is $c_L = 0.79_{-0.1}^{+0.05}$ for $R < 16''$ (0.82 kpc), flattening beyond this point and reaching $c_L = 0.66_{-0.08}^{+0.07}$ at $R = 38''$ (1.9 kpc). The results are similar, with slightly steeper gradients in T and c_L , if the galaxy is assumed *a priori* to rotate about its short axis. While the estimates for c_L are robust, those for T are dependent on the degree to which the internal rotation field is disklike or spheroid-like. There are regions in the dynamical parameter space where the preferred shapes are prolate-triaxial. Thus the triaxiality estimate should not be considered robust until the dynamical prior can be better constrained on physical grounds.

The inclination of the short axis to the line of sight is not well determined, because the triaxiality is not well determined. Inclinations between 30° and 50° are preferred. However, highly triaxial models in high inclination are also allowed, which can affect central black hole mass estimates (Magorrian et al. 1998, G00) by factors of a few. The position angle of the projected short axis on the sky is well constrained, and lies within 10° of the photometric minor axis at better than 3σ confidence. Similar, though weaker, constraints can be placed on the P.A. and inclination of the long axis. These constraints rule out the possibility that the nuclear dust ring at $R \approx 1''.5$ lies in one of the planes normal to either axis. Stable equilibria for planar gas disks in triaxial potentials exist only in these planes. Alternatively, if $T \equiv 0$ and the short axis inclination is

< 43° (3 σ limit), the dust could be in a neutrally stable equilibrium in a polar ring. However, even in this configuration the ring would be torqued by dynamical friction against the rotating stellar population, which would act toward aligning the ring with the stellar rotation axis. The ring is clearly a *decoupled nuclear component* whose orientation is not linked to the main body of the galaxy.

The dust ring may be connected with the ionized gas that extends out to $R \approx 8''$ (Macchetto et al. 1996, P00). The projected gas rotation axis is near the minor axis of the ring, though the H α +[N II] isophotes are very round. It is possible that the gas and dust are both part of a strongly warped disk. However, the evolution and expected lifetime of such a structure are problematic. If the warp is caused by differential precession, one should expect the entire structure to wind up on itself in $\sim 10^7$ years. The decoupling with the stellar component would suggest that the gas has an external origin. But no trace of recent interaction or accretion is seen at larger radii, where it would presumably be much longer lived. At very large radii ($\gtrsim 10'$), NGC 3379 and NGC 3384 are collectively surrounded by a ring of H I (Schneider 1985) whose connection with these and neighboring galaxies is far from clear (Schneider 1989). Whether the intergalactic ring could be a source of material for occasional accretion events, and how this material might evolve dynamically as it accreted into the nuclear regions, are topics for future work.

Many thanks to Karl Gebhardt for providing data in advance of publication and for helpful comments. An anonymous referee also kindly suggested several improvements to the paper. This work was supported by NSF CAREER grant AST-9703036.

REFERENCES

Ajhar, E. A., Lauer, T. R., Tonry, J. L., Blakeslee, J. P., Dressler, A., Holtzman, J. A., & Postman, M. 1997, AJ, 114, 626

Arnaboldi, M. & Sparke, L. S. 1994, AJ, 107, 958

Bak, J. & Statler, T. S. 2000, AJ, 120, 110 (BS)

Bender, R., Saglia, R. P., & Gerhard, O. E. 1994, MNRAS, 269, 785

Capaccioli, M., Held, E. V., & Nieto, J.-L. 1987, AJ, 94, 1519

Capaccioli, M., Vietri, M., Held, E. V., & Lorenz, H. 1991, ApJ, 371, 535

Carollo, C. M., Franx, M., Illingworth, G. D., & Forbes, D. A. 1997, ApJ, 481, 710

Ciardullo, R., Jacoby, G. H., & Dejonghe, H. B. 1993, ApJ, 414, 454

Davies, R. L. & Birkinshaw, M. 1988, ApJS, 68, 409

Davies, R. L. & Illingworth, G. 1983, ApJ, 266, 516

de Vaucouleurs, G. & Capaccioli, M. 1979, ApJS, 40, 699

Ferrarese, L. & Merritt, D. 2000, ApJ539, L9

Fisher, D. 1997, AJ, 113, 950

Gebhardt, K. & Richstone, D. 2000, in preparation.

Gebhardt, K., Richstone, D., Kormendy, J., Lauer, T. R., Ajhar, E. A., Bender, R., Dressler, A., Faber, S. M., Grillmair, C., Magorrian, J., & Tremaine, S. 2000a, AJ, 119, 1157 (G00)

Gebhardt, K., Bender, R., Bower, G., Dressler, A., Faber, S. M., Filippenko, A. V., Green, R., Grillmair, C., Ho, L. C., Kormendy, J., Lauer, T. R., Magorrian, J., Pinkney, J., Richstone, D., & Tremaine, S. 2000b, *ApJ*, 539, L13

Goudfrooij, P., Hansen, L., Jørgensen, H. E., Nørgaard-Nielsen, H. U., De Jong, T., & van den Hoek, L. 1994, *A&AS*, 104, 179

Macchetto, F., Pastoriza, M., Caon, N., Sparks, W. B., Giavalisco, M., Bender, R., & Capaccioli, M. 1996, *A&AS*, 120, 463

Magorrian, J., Tremaine, S., Richstone, D., Bender, R., Bower, G., Dressler, A., Faber, S. M., Gebhardt, K., Green, R., Grillmair, C., Kormendy, J., & Lauer, T. 1998, *AJ*, 115, 2285.

Michard, R. 1998, *A&A*, 334, 453

Pastoriza, M. G., Winge, C., Ferrari, F., Macchetto, F. D., & Caon, N. 2000, *ApJ*, 529, 866 (P00)

Peletier, R. F., Davies, R. L., Davis, L. E., Illingworth, G. D., & Cawson, M. 1990, *AJ*, 100, 1091

Ryden, B. S. 1992, *ApJ*, 396, 445

Sackett, P. D., Rix, H.-W., Jarvis, B. J., & Freeman, K. C. 1994, *ApJ*, 436, 629

Schneider, S. 1985, *ApJ*, 288, L33

Schneider, S. 1989, *ApJ*, 343, 94

Schweizer, F. & Seitzer, P. 1992, *AJ*, 104, 1039

Sparke, L. S. 1986, *MNRAS*, 219, 657

Statler, T. S. 1994a, *ApJ*, 425, 458 (Paper I)

Statler, T. S. 1994b, *ApJ*, 425, 500 (Paper III)

Statler, T. S. 1994c, *AJ*, 108, 111 (S94)

Statler, T. S., Dejonghe, H., & Smecker-Hane, T. 1999, *AJ*, 117, 126 (SDS)

Statler, T. S. & Fry, A. M. 1994, *ApJ*, 425, 481 (Paper II)

Statler, T. S., & Smecker-Hane, T. 1999, *AJ*, 117, 839 (SS99)

Statler, T. S., Smecker-Hane, T., & Cecil, G. 1996, *AJ*, 111, 1512

van der Marel, R. P., Binney, J. J., & Davies, R. L. 1990, *MNRAS*, 245, 582

van Dokkum, P. G. & Franx, M. 1995, *AJ*, 110, 2027

Whitmore, B. C., Lucas, R. A., McElroy, D. B., Steiman-Cameron, T. Y., Sackett, P. D., & Olling, R. P. 1990, *AJ*, 100, 1489